INSTITUTE FOR FUSION STUDIES

DOE/ET-53088-543 IFSR #543

Kinetic Theory of Toroidicity-Induced Alfvén Eigenmodes

R.R. METT and S.M. MAHAJAN
Institute for Fusion Studies
The University of Texas at Austin
Austin, Texas 78712

March 1992

THE UNIVERSITY OF TEXAS

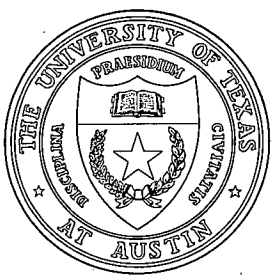

AUSTIN

Kinetic Theory of Toroidicity-Induced Alfvén Eigenmodes

R. R. Mett and S. M. Mahajan
Institute for Fusion Studies
The University of Texas at Austin
Austin, Texas 78712

Abstract

An analytic kinetic description of the toroidicity-induced Alfvén eigenmode (TAE) is presented. The theory includes electron parallel dynamics non-perturbatively, an effect which is found to strongly influence the character and damping of the TAE — contrary to previous theoretical predictions. We use a parallel conductivity model that includes collisionless (Landau) damping on the passing electrons and collisional damping on both trapped and passing electrons. Together, these mechanisms damp the TAE more strongly than previously expected. This is because the TAE couples (or merges) with the kinetic Alfvén wave (KAW) under conditions which depend on the gap size, the shear, the magnitude of the conductivity and the mode numbers. The high damping could be relevant to recent experimental measurements of the TAE damping coefficient. In addition, the theory predicts a "kinetic" TAE, whose eigenfrequency lies just above the gap, whose existence depends on finite conductivity, and which is formed by the coupling of two KAWs.

PACS numbers: 51.10.+y, 52.40.Db

I. Introduction

Toroidicity-induced Alfvén eigenmodes (TAE) are currently of great interest because they may destroy the confinement of fast ions in a burning tokamak plasma.[1–9] Their excitation depends critically on the difference between the growth rate due to the fast ions and the damping rate, mainly due to electrons. Past theories have predicted a very low intrinsic damping for the TAE,[2,3] and have determined the dominant form to be Landau damping due to the magnetic curvature drift of the electrons.[2] Perhaps stimulated by recent Tokamak Fusion Test Reactor (TFTR)[4,10] and Doublet III-D (DIII-D)[5,11] results showing a higher excitation threshold than expected, more recent theoretical studies have focused on alternate damping mechanisms, such as continuum damping,[6–8] and trapped electron effects.[9] In contrast, the present study attempts to demonstrate that a non-perturbative treatment of electron parallel dynamics yields intrinsic damping of the TAE significantly higher than originally thought.

The higher damping is caused by a coupling between (or merging together of) the TAE and the kinetic Alfvén wave (KAW) if the gap is sufficiently thin and/or the magnitude of the conductivity is sufficiently small. In this regime, the damping is strong and relatively insensitive to the real part of the parallel conductivity σ because the KAW carries the energy of the mode away from the gap region. Outside this regime, as previously predicted, the TAE damping depends linearly on the real part of σ^{-1}, and may be quite small. Our theory also points out interesting connections between the TAE and the global Alfvén eigenmode[12–14] (GAE). In addition to altering the structure of the TAE, finite conductivity introduces a countable infinity of new modes (like for the GAE[12]), which are formed by the coupling between two KAWs. These new modes, which we call kinetic TAE (KTAE), have eigenfrequencies which lie just above the gap. Their damping scales as $\sigma^{-1/2}$. We find that

the KTAE closest to the gap has a mode structure very similar to the TAE, but with the opposite phase between the coupled modes, and may have a lower damping coefficient than the TAE. The modes further outside the gap generally have high damping coefficients. The KTAE correspond to the continuum, which has been discretized by the electron dynamics. Analytical calculations of the dispersion relations and damping coefficients for the various modes in various regimes are in good agreement with numerical values obtained by direct integration of the basic equations for a wide range of plasma parameters.

The paper is organized as follows. Section II contains a derivation of the basic coupled set of equations used to describe the TAE and KTAE. Properties of the system in the ideal magnetohydrodynamic (MHD) limit are examined in Sec. III. Analytic dispersion relations for the modes in various parameter regimes are derived using a variational approach in Sec. IV. In Sec. V, numerical results obtained by direct integration of the coupled set of equations are presented and discussed, while conclusions are given in Sec. VI.

II. Basic Equations

We consider a TAE formed by the coupling between two poloidal harmonics m_1 and m_2. As our model, we use an equation describing Alfvén waves in an inhomogeneous, current carrying, cylindrical plasma, corrected by toroidal coupling to first order in inverse aspect ratio $\varepsilon(r) = r/R$,

$$\left[rK_1^2\frac{d}{dr}\frac{\Delta_1}{rK_1^2}\frac{d}{dr}r - rK_1^2(\Delta_1 - G_1) + K_1k_1\left(\frac{d}{dr}r\frac{d}{dr} - rK_1^2\right)\frac{\tau_1}{K_1k_1}\left(\frac{1}{r^2}\frac{d}{dr}r\frac{d}{dr}r - K_1^2\right)\right]E_1$$

$$= -2\left(\frac{d}{dr}\varepsilon\frac{\omega^2}{v_A^2}\frac{d}{dr} - K_2^2\varepsilon\frac{\omega^2}{v_A^2}\right)rE_2\ . \qquad (1)$$

In this equation, the poloidal electric field $E(r) \sim e^{i(m\theta+n\phi-\omega t)}$, the poloidal wavenumber $K = (q^2+\varepsilon^2)^{-1/2}(mq+\varepsilon^2 n)/r$, the parallel wavenumber $k = (q^2+\varepsilon^2)^{-1/2}(m-nq)/R$, while $\Delta = \omega^2/v_A^2 - k^2, G = (dA/dr)/K - A^2/K^2$, where $A = \varepsilon(2qk - \varepsilon K)/[r(q^2+\varepsilon^2)]$, and τ is

related to the parallel conductivity σ as

$$\tau = \frac{-i\omega}{\sigma\mu_0 v_A^2} . \tag{2}$$

The coupled system is completed with the equation formed by exchanging the subscripts $1 \leftrightarrow 2$. The left-hand side of this equation was derived in Ref. 12 and used to examine KAW and GAE.[12-14] It stems from the well-known system of equations describing Alfvén waves derived in Ref. 15. Electron dynamics are described by the term containing τ, while G contains the effect of shear or equilibrium current [$G \sim \pm s$ where $s = dlnq/dlnr$; to leading order in ε, $G = (dk^2/dr)/(rK^2)$]. We note that the toroidal coupling term on the right-hand side of Eq. (1) is the same as Eq. (30) of Ref. 1. Neglecting the term containing τ, Eq. (1), apart from the last term on the right-hand side, is the same as Eq. (35) of Ref. 8. Equation (1) may also be reduced to Eq. (2) of Ref. 7 under appropriate limits. We have taken the toroidal coupling strength in Eq. (1) to be $2\frac{r}{R}$. This is because, heuristically, half of this comes from the variation of ω^2/v_A^2 with θ through $R = R_0(1 + \epsilon\cos\theta)$ and half comes from the variation of k^2 with θ through R. Other works have used a value of $2.5\frac{r}{R}$,[6-8] where the additional 1/2 comes from a Shafranov shift in the equilibrium,[8] which we do not consider. We point out that there are, in addition, many other ϵ-dependent terms which come from the equilibrium, and keeping some of these may not be entirely justifiable. Our results, however, are changed little if the additional 0.5 were included.

Our parallel conductivity model includes collisionless (Landau) damping on passing electrons and collisional damping on both trapped and passing electrons. It was derived by following the drift-tearing mode analysis of Chen, Rutherford and Tang,[16] except we have added a particle conserving Krook collision operator for the passing electrons on the ions. The derivation is outlined in the Appendix. We find

$$\tau = \frac{k^2\rho_s^2}{F} , \tag{3}$$

where $\rho_s = c_s/\omega_{ci}$ and

$$F = \left\{ \frac{1-(2\varepsilon)^{1/2}+\zeta[Z(\zeta)-Z(\zeta_t)]}{1-(2\varepsilon)^{1/2}+\zeta_c[Z(\zeta)-Z(\zeta_t)]}[1-(2\varepsilon)^{1/2}] \right\} \{1+B_1\} \ . \tag{4}$$

The variable F factors into a passing particle contribution (coming from an integral over the passing electrons), given by the first term in curly braces, and a trapped particle contribution (coming from an integral over the trapped electrons), which is purely collisional, given by the last term. Here, Z is the plasma dispersion function, $\zeta = (\omega + i\nu_p)/(|k|v_e)$, $\zeta_t = \zeta/(2\varepsilon)^{1/2}$, $\zeta_c = i\nu_p/(|k|v_e)$, where ν_p is an effective collision frequency for the passing electrons on the ions and v_e is the electron thermal speed, while

$$B_1 = \frac{(2\varepsilon)^{1/2}}{1-(2\varepsilon)^{1/2}} \frac{4}{\pi^{1/2}} \int_0^\infty dx\, x^2 e^{-x^2} \frac{i\nu(x)}{\omega + i\nu(x)} \ . \tag{5}$$

In Eq. (5), $\nu(x) = (\nu_e/\varepsilon)x^{-3}$ where ν_e is the collision frequency of thermal electrons on the ions. We comment that F reduces to Eq. (9) of Ref. 16 in the limit $\nu_p \to 0$ (and for $\omega_*/\omega \to 0$). It also takes the form reported in Eq. (30) of Mahajan, Hazeltine, Strauss, and Ross for $\varepsilon \to 0$.[17] In this limit the conductivity becomes the Spitzer conductivity for $\nu_p/(|k|v_e) \gg 1$ and describes collisionless Landau damping [$F = 1 + \zeta Z(\zeta)$] for $\nu_p \ll \omega$. Equations (2) and (3) may be combined to yield a more familiar relation,

$$\sigma = -i\frac{ne^2}{T_e}\frac{\omega}{k^2}F \ , \tag{6}$$

where n is the plasma density, e is the unit charge and T_e is the electron temperature. For typical plasma parameters, F is of order unity. Neglecting collisions, the trapped particles (by removing a cone of passing electrons from velocity space) tend to decrease slightly the real part of F and decrease substantially the imaginary part to a small fraction of the real part. Collisions have their largest effect on the imaginary part of F, increasing it to a significant fraction of the real part for typical plasma parameters.

The essential features of the TAE may be obtained from Eq. (1) and its counterpart by expanding $\Delta(r)$ in powers of r about the position r_0 where $\Delta_1 = \Delta_2$. For simplicity we

assume the radial variation in all other quantities (except E) about r_0 is unimportant. We take $\phi(r) = rE(r)$, $r = r_0 + x$, $\Delta_1 = \Delta - \alpha_1 x$, $\Delta_2 = \Delta + \alpha_2 x$, where $\alpha_1 = -d\Delta_1/dr|_{r_0}$, $\alpha_2 = d\Delta_2/dr|_{r_0}$ and obtain

$$\left[\frac{d}{dx}(\Delta - \alpha_1 x)\frac{d}{dx} - K_1^2(\Delta - \alpha_1 x - G_1) + \tau\left(\frac{d^2}{dx^2} - K_1^2\right)^2\right]\phi_1 = -2\varepsilon\frac{\omega^2}{v_A^2}\left(\frac{d^2}{dx^2} - K_2^2\right)\phi_2 \ . \tag{7}$$

The other equation has $1 \leftrightarrow 2$ and the opposite sign of α. Here, the quantities $\Delta, \tau, \varepsilon, v_A, K_1, K_2, G_1, G_2$ are all evaluated at $r = r_0$ and are therefore constants. (The subscripts were dropped on Δ and τ since $1 = 2$.)

Equation (7) and its counterpart are conveniently analyzed in Fourier space. Parseval's theorem implies that any function localized (square integrable) in x will also be localized in the conjugate Fourier variable. We take

$$\phi(x) = \int_{-\infty}^{\infty} dp\tilde{\phi}(p)e^{ipx} \tag{8a}$$

$$\tilde{\phi}(p) = \frac{1}{2\pi}\int_{-\infty}^{\infty} dx\phi(x)e^{-ipx} \tag{8b}$$

and Eq. (7) becomes

$$\left[\frac{d}{dp} + \frac{i\Delta}{\alpha_1} + \frac{p}{p^2 + K_1^2} - \frac{iK_1^2 G_1}{\alpha_1(p^2 + K_1^2)} - \frac{i\tau}{\alpha_1}(p^2 + K_1^2)\right]\tilde{\phi}_1 = -\frac{2i\varepsilon}{\alpha_1}\frac{\omega^2}{v_A^2}\frac{p^2 + K_2^2}{p^2 + K_1^2}\tilde{\phi}_2 \ . \tag{9}$$

This equation and its counterpart may be symmetrized by defining the new functions

$$\psi_1 = \tilde{\phi}_1[\alpha_1 e^{i\eta}(p^2 + K_1^2)]^{1/2} \tag{10a}$$

$$\psi_2 = \tilde{\phi}_2[\alpha_2 e^{i\eta}(p^2 + K_2^2)]^{1/2} \tag{10b}$$

where $\eta = (\alpha_1^{-1} - \alpha_2^{-1})(\Delta p - \frac{1}{3}\tau p^3) - \tau(K_1^2/\alpha_1 - K_2^2/\alpha_2)p - K_1 G_1 \alpha_1^{-1}\,\mathrm{atan}\left(\frac{p}{K_1}\right) + K_2 G_2 \alpha_2^{-1}\,\mathrm{atan}\left(\frac{p}{K_2}\right)$. Then Eq. (9) and its counterpart reduce to the simple normalized system

$$\left[\frac{d}{dy} + ih(y)\right]\psi_1 = -i\hat{\varepsilon}\psi_2 f(y) \ , \tag{11a}$$

$$\left[\frac{d}{dy} - ih(y)\right]\psi_2 = \frac{i\hat{\varepsilon}\psi_1}{f(y)} , \tag{11b}$$

where the normalized Fourier coordinate $y = p/\kappa$, the normalized inverse aspect ratio $\hat{\varepsilon} = 2\varepsilon\kappa(\alpha_1\alpha_2)^{-1/2}\omega^2/v_A^2$, while the functions $h(y) = \hat{\Delta} - \hat{G}(y) - \hat{\tau}(y^2+1)$, and $f(y) = [(y^2 + y_2^2)/(y^2+y_1^2)]^{1/2}$. Here, the normalized eigenvalue $\hat{\Delta} = \frac{1}{2}\kappa\Delta/\alpha$, the normalized "shear" parameter $\hat{G}(y) = \frac{1}{2}[\hat{G}_1/(1+y^2/y_1^2) + \hat{G}_2/(1+y^2/y_2^2)]$, and the normalized inverse parallel conductivity $\hat{\tau} = \frac{1}{2}\tau\kappa^3/\alpha$, where $\kappa = [\alpha(K_1^2/\alpha_1 + K_2^2/\alpha_2)]^{1/2}$, $\alpha = (\alpha_1^{-1} + \alpha_2^{-1})^{-1}$, $\hat{G}_1 = \kappa G_1/\alpha_1$, $\hat{G}_2 = \kappa G_2/\alpha_2$, $y_1 = K_1/\kappa$, and $y_2 = K_2/\kappa$. We have reduced the TAE problem to a coupled pair of linear, first order, ordinary differential equations with the eigenvalue ω entering through $\hat{\Delta}(\omega)$, $\hat{\tau}(\omega)$, and $\hat{\varepsilon}(\omega)$. For the TAE, we expect $\hat{\Delta}(\omega)$ to be small ($\hat{\Delta} \sim \hat{\varepsilon}$) and so it is a good approximation to put $\hat{\tau}(\omega) = \hat{\tau}(kv_A)$ and $\hat{\varepsilon}(\omega) = \hat{\varepsilon}(kv_A)$ and treat $\hat{\Delta}$ as the eigenvalue. It is clear from the definition of $h(y)$ that since $\hat{\tau}$ is small, it will influence only the high frequency (in p or y) components of the wave function, as expected. In terms of the normalized variables, the eigenfrequency is given by

$$\omega = kv_A\left[1 + 4\varepsilon\frac{(m_1m_2)^{1/2}}{m_1+m_2}\left(\frac{\hat{\Delta}}{\hat{\varepsilon}}\right)\right]^{1/2} , \tag{12}$$

and so the damping is, to leading order in ε,

$$\frac{\gamma}{\omega} = 2\varepsilon\frac{(m_1m_2)^{1/2}}{m_1+m_2}\,\mathrm{Im}\left(\frac{\hat{\Delta}}{\hat{\varepsilon}}\right) , \tag{13}$$

and the gap boundary

$$\hat{\Delta}_{\mathrm{gap}} = \pm\hat{\varepsilon}\frac{m_1+m_2}{2(m_1m_2)^{1/2}} . \tag{14}$$

III. Existence of TAE in Ideal MHD Limit

Before solving Eqs. (11a) and (11b), it is illuminating to examine properties of the system with $\hat{\tau} = 0$. Then these equations may be combined into

$$\left\{\frac{d}{dy}f\frac{d}{dy} + f\left[(\hat{\Delta}-\hat{G})^2 - \hat{\varepsilon}^2\right] - i\frac{d}{dy}\left[f(\hat{\Delta}-\hat{G})\right]\right\}\psi_2 = 0 . \tag{15}$$

Since $f(y)$, $\widehat{G}(y)$, $\widehat{\varepsilon}$ are all real, we expect $\widehat{\Delta}$ to be real. Since $f(y) \to 1$ and $\widehat{G}(y) \to 0$ as $y \to \infty$, asymptotically Eq. (15) becomes

$$\left[\frac{d^2}{dy^2} + (\widehat{\Delta}^2 - \widehat{\varepsilon}^2)\right] \psi_2 = 0 \ . \tag{16}$$

Consequently for a bounded solution, $\widehat{\Delta}^2 - \widehat{\varepsilon}^2 < 0$. Taking the inner product $\langle\rangle = \int_{-\infty}^{\infty} dy$ of Eq. (15) with ψ_2^* and adding the result to its complex conjugate, we find

$$(\widehat{\Delta}^2 - \widehat{\varepsilon}^2) \left\langle f|\psi_2|^2 \right\rangle = \left\langle f \left|\frac{d\psi_2}{dy}\right|^2 \right\rangle - \left\langle f\widehat{G}(\widehat{G} - 2\widehat{\Delta})|\psi_2|^2 \right\rangle \ . \tag{17}$$

Since $f(y)$ is positive for all y, this (virial-type) equation shows that finite $\widehat{G}(y)$ is required to make $\widehat{\Delta}^2 - \widehat{\varepsilon}^2 < 0$ and thus to create a localized mode. The function $f(y)$ plays essentially no role in the formation of the mode. Consequently, with no parallel electric field ($\widehat{\tau} = 0$), equilibrium current (essential for the GAE[12–14]) and toroidal coupling are both essential for the formation of the TAE. The function $\widehat{G}(y)$ plays a similar role as boundary conditions in other analyses.[1,7,8] Notice also that since $\widehat{\varepsilon}$ is small, it is quite likely that there is only a single mode — one with no nodes (zero crossings) in ψ_2. This is because as one creates a node, $|d\psi_2/dy|^2$ increases, requiring $|\widehat{\Delta}|$ to increase (on the right-hand side), but thereby preventing $\widehat{\Delta}^2 - \widehat{\varepsilon}^2 < 0$. It is also seen that a larger $|\widehat{G}(y)|$ requires a larger $|d\psi_2/dy|^2$ and a smaller $|\psi_2|^2$, which implies a more localized mode in y-space (and thus a broader mode in x-space). These tendencies are born out in the numerical solutions of Eqs. (11a) and (11b), presented in Sec. V.

If the K_1^2 and K_2^2 terms are dropped in the coupling terms on the right-hand side of Eq. (7) and its counterpart (often used as an approximation), a similar virial-type construction shows that a finite $\widehat{G}(y)$is *not* required to make $\widehat{\Delta}^2 - \widehat{\varepsilon}^2 < 0$. It indicates, incorrectly, that a TAE may be formed by toroidal coupling alone. Since it is more accurate to keep the K_1^2 and K_2^2 terms, this suggests that many terms are of the same order and so one must be cautious when dropping various terms.

Finally, we point out that with $\hat{\tau} \neq 0$ the condition $\hat{\Delta}^2 - \hat{\varepsilon}^2 < 0$ is no longer necessary to permit a localized solution.

IV. Analytic Dispersion Relations

We now analytically derive the dispersion relations and damping coefficients using a variational technique. Two distinct modes emerge from the analysis. One, the TAE, persists in the limit $\hat{\tau} \to 0$. The other, the KTAE, does not. For $\hat{\tau}$ sufficiently small, the damping of the TAE is scales as $\mathrm{Im}(\hat{\tau})$, but may be enhanced significantly by $\hat{\varepsilon}$ and $\hat{G}$. For larger $\hat{\tau}$, the damping depends on the magnitude of $\hat{\tau}$ and becomes relatively insensitive to $\mathrm{Im}(\hat{\tau})$. For the KTAE the damping scales as $\hat{\tau}^{1/2}$. Analytical results are in good agreement with values obtained by direct numerical integration of the basic equations.

Recognizing from the arguments of the previous section that $f(y)$ plays a minimal role in the form of the TAE, for simplicity we set $f(y) = 1$ in Eqs. (11a) and (11b). We further make the simplification $\hat{G}(y) \cong \hat{G}_0/(y^2+1)$, where $\hat{G}_0 = \frac{1}{2}(\hat{G}_1 + \hat{G}_2)$ (generally $\hat{G}_0 > 0$). This makes $h(y)$ symmetric in y. From our numerical solutions of Eqs. (11a) and (11b), we observe for the TAE that

$$\psi_2(y) \cong \psi_1(-y) \ , \tag{18a}$$

to a good approximation, while for the KTAE

$$\psi_2(y) \cong -\psi_1(-y) \ . \tag{18b}$$

Substituting Eq. (18a) into Eqs. (11a) and (11b) with our simplifications, we form a coupled system for symmetric and antisymmetric functions defined by $\psi_s(y) = \psi_1(y) + \psi_1(-y)$ and $\psi_a(y) = \psi_1(y) - \psi_1(-y)$. This system may then be combined into a single equation for ψ_s,

$$\frac{d}{dy}\left[\frac{1}{\hat{\varepsilon} - h_0(y)}\frac{d\psi_s}{dy}\right] - [\hat{\varepsilon} + h_0(y)]\psi_s = 0 \ , \tag{19}$$

where $h_0(y) = \hat{\Delta} - \hat{G}_0/(y^2+1) - \hat{\tau}(y^2+1)$. A similar procedure using Eq. (18b) for the KTAE leads to Eq. (19) with $\hat{\varepsilon}$ replaced by $-\hat{\varepsilon}$. [Equations (11a) and (11b) may also be combined into a single (Schrödinger) equation, $\psi_2'' + V\psi_2 = 0$, where the effective potential $V(y) = h_0^2 - \hat{\varepsilon}^2 - i dh_0/dy$. It is interesting to note the similarity between $h_0(y)$ and the effective potential for the GAE discussed in Ref. 12 — c.f. Eqs. (23) and (24) and Figs. 1 and 2. However, the correspondence is not complete since in the present case the effective potential is significantly more complicated.]

In leading up to our variational procedure, we take the inner product of Eq. (19) with ψ_s to obtain the quadratic form

$$S = I_1 + I_2 = 0 \ , \tag{20}$$

where $I_1 = -\left\langle \frac{1}{\hat{\varepsilon}-h_0(y)} \left(\frac{d\psi_s}{dy}\right)^2 \right\rangle$ and $I_2 = -\langle [\hat{\varepsilon} + h_0(y)]\psi_s^2 \rangle$. We take the trial function $\psi_s = e^{-\lambda y^2/2}$ with the (complex) parameter λ, substitute into Eq. (20), and carry out the integrals. Perhaps surprisingly, the integrals may be carried out exactly and written in terms of the probability integral Φ.[18] We find

$$I_1 = \frac{-\lambda^2}{\hat{\tau}(z_+ - z_-)} \left[I_+ - I_- - \frac{\partial}{\partial \lambda}(I_+ - I_-) \right] \ , \tag{21}$$

$$I_2 = -(\hat{\varepsilon} + \hat{\Delta}) \left(\frac{\pi}{\lambda}\right)^{1/2} + \pi \hat{G}_0 e^{\lambda} [1 - \Phi(\lambda^{1/2})] + \hat{\tau} \left(\frac{\pi}{\lambda}\right)^{1/2} \left(1 + \frac{1}{2\lambda}\right) \ , \tag{22}$$

where

$$I_\pm = \left(\frac{\pi}{\lambda}\right)^{1/2} - \pi (1 - z_\pm)^{1/2} e^{\lambda(1-z_\pm)} \left\{ 1 - \Phi[(1-z_\pm)^{1/2}\lambda^{1/2}] \right\} \ , \tag{23}$$

$$z_\pm = \frac{\hat{\Delta} - \hat{\varepsilon}}{2\hat{\tau}} \left\{ 1 \pm \left[1 - \frac{4\hat{\tau}\hat{G}_0}{(\hat{\varepsilon} - \hat{\Delta})^2} \right]^{1/2} \right\} \ . \tag{24}$$

The integrals are strictly valid for $|\mathrm{Arg}(\lambda^{1/2})| < \frac{\pi}{4}$ and $\mathrm{Re}[(1-z_\pm)^{1/2}] > 0$.

We now take advantage of the ordering of the various terms. In general, $|\hat{\tau}| \ll |\hat{\Delta}| \sim |\hat{\varepsilon}| \ll 1$, while $0 < \hat{G}_0 < 1$ and $|\lambda| \ll 1$. Then

$$z_+ \cong \frac{\hat{\Delta} - \hat{\varepsilon}}{\hat{\tau}} \ , \tag{25}$$

$$z_- \cong \frac{\widehat{G}_0}{\widehat{\Delta} - \widehat{\varepsilon}} \,. \tag{26}$$

Consequently, $|z_+| \gg 1 \sim |z_-|$. If $\widehat{\tau}$ is sufficiently small, z_+ becomes sufficiently large that we can use the asymptotic expansion of Φ to evaluate I_+. Then to leading order in $\lambda^{-1/2}$,

$$I_+ = \frac{\pi^{1/2}}{2(1 - z_+)\lambda^{3/2}} \,. \tag{27}$$

Since λ is small and z_- is of order unity, we can use the small argument expansion of Φ to determine I_-. To leading order

$$I_- = \left(\frac{\pi}{\lambda}\right)^{1/2} \,. \tag{28}$$

With these results,

$$I_1 = \frac{(\pi\lambda)^{1/2}}{2(\widehat{\Delta} - \widehat{\varepsilon})} \,, \tag{29}$$

and our quadratic form Eq. (20) becomes

$$S = \frac{\widehat{\tau}}{2\lambda} - \widehat{\varepsilon} - \widehat{\Delta} + \widehat{G}_0(\pi\lambda)^{1/2} - \frac{\lambda}{2(\widehat{\varepsilon} - \widehat{\Delta})} = 0 \,. \tag{30}$$

The parameter λ is determined by finding the extremum of Eq. (30), which corresponds to a solution of $\partial S/\partial\lambda = 0$, or

$$-\frac{\widehat{\tau}}{\lambda^2} + \widehat{G}_0 \left(\frac{\pi}{\lambda}\right)^{1/2} - \frac{1}{\widehat{\varepsilon} - \widehat{\Delta}} = 0 \,. \tag{31}$$

If $\widehat{\tau}$ is sufficiently small, an accurate solution of Eq. (31) may be obtained by solving perturbatively in $\widehat{\tau}$,

$$\lambda^{1/2} = \frac{\pi^{1/2}\widehat{G}_0(\widehat{\varepsilon} - \widehat{\Delta})}{1 + \widehat{\tau}/[\pi\widehat{G}_0^2(\widehat{\varepsilon} - \widehat{\Delta})]} \,. \tag{32}$$

[We comment that the solution neglecting $\widehat{G}_0$ does not satisfy the constraints on the integrals.] Substituting this into Eq. (30) gives the dispersion relation

$$\widehat{\Delta} = -\widehat{\varepsilon}\frac{1 - \pi\widehat{G}_0^2/2}{1 + \pi\widehat{G}_0^2/2} + \frac{\widehat{\tau}}{2\pi\widehat{G}_0^2(\widehat{\varepsilon} - \widehat{\Delta})^2(1 + \pi\widehat{G}_0^2/2)} \,. \tag{33}$$

This shows that for $\hat{\tau} = 0$, $\hat{\Delta}^2 < \hat{\varepsilon}^2$ in accord with the results from the previous section. Furthermore, for $|\hat{\tau}/(8\pi\hat{G}_0^2\hat{\varepsilon}^2)| \ll \hat{\varepsilon}$, $\mathrm{Im}(\hat{\Delta}) \sim \mathrm{Im}(\hat{\tau})$. Consequently [see Eq. (13)] the damping coefficient is proportional to $\mathrm{Im}(\hat{\tau})$ and is enhanced by the small parameters $\hat{\varepsilon}$ and $\hat{G}_0$. Iterative solutions of Eq. (33) show that as $|\hat{\tau}/(8\pi\hat{G}_0^2\hat{\varepsilon}^2)| \sim \hat{\varepsilon}$, $\mathrm{Im}(\hat{\Delta})$ increases dramatically with $|\hat{\tau}|$. This is shown in Fig. 1a, where Eq. (33) is labelled "33." The solid lines indicate the real part and the dashed lines the negative imaginary part of $(\hat{\Delta}/\hat{\varepsilon} + 1)$, plotted as a function of $|\hat{\tau}|/\hat{\varepsilon}^3$ over several decades. The (representative) values $\hat{\varepsilon} = 0.1$, $\hat{G}_0 = 0.3$, and $\mathrm{Arg}(\hat{\tau}) = -0.3$ were used. The rapid increase in $\mathrm{Im}(\hat{\tau})$ is also reflected in the numerical solution of Eqs. (11a) and (11b), labelled "C" in Fig. 1a, although the increase is a bit more gradual and begins for smaller $|\hat{\tau}|/\hat{\varepsilon}^3$. As $|\hat{\tau}/(8\pi\hat{G}_0^2\hat{\varepsilon}^2)| \sim \hat{\varepsilon}$, our approximations begin to break down and $\mathrm{Re}(\hat{\Delta})$ predicted by Eq. (33) diverges from its true value.

The TAE root may be traced further by going back to Eq. (23) and using the small argument expansion of Φ to determine I_+ (since $|z_+|$ is reduced by larger $\hat{\tau}$). Then

$$I_1 = \frac{\pi^{1/2}\lambda^{3/2}}{\hat{\tau}} , \tag{34}$$

and our quadratic form Eq. (20) becomes

$$S = \frac{\hat{\tau}}{2\lambda} - \hat{\varepsilon} - \hat{\Delta} + \hat{G}_0(\pi\lambda)^{1/2} - \frac{\lambda^2}{\hat{\tau}} = 0 . \tag{35}$$

The extremum of this equation which satisfies the conditions on the integrals is, to a good approximation,

$$\lambda = \left(\frac{i\hat{\tau}}{2}\right)^{2/3} , \tag{36}$$

and gives the dispersion relation

$$\hat{\Delta} = -\hat{\varepsilon} - \left(\frac{3i}{2}\right)\left(\frac{i\hat{\tau}}{2}\right)^{1/3} . \tag{37}$$

[In this equation and all subsequent discussion, only the primary root (the one with smallest absolute value of argument) is implied. The other roots do not satisfy the constraints on the

integrals. Note in Eq. (37) that the argument of $\hat{\tau}$ still makes $-\hat{\varepsilon} < \mathrm{Re}(\hat{\Delta}) < 0$, which is also true for Eq. (33).] This result is independent of $\hat{G}_0$, suggesting that the electron dynamics in some sense dominate over the MHD effects as $\hat{\tau}$ becomes sufficiently large. Equation (37) is plotted in Fig. 1a and labelled "37." Note the surprising continuity in $\mathrm{Im}(\hat{\Delta})$ from Eq. (33) to Eq. (37) as $|\hat{\tau}|/\hat{\varepsilon}^3$ increases. Taken together, these dispersion relations follow $\mathrm{Im}(\hat{\Delta})$ determined by numerical solution of Eqs. (11a) and (11b) within a factor of two or three. The real and imaginary parts of $\hat{\Delta}$ from Eq. (37) agree well with the code for $|\hat{\tau}|/\hat{\varepsilon}^3 > 10$. The correspondence is good considering the simplifications and approximations used. Equation (37) also has the surprising feature that the damping does not vanish as $\mathrm{Im}(\hat{\tau}) \to 0$. This is because in this regime TAE is dominated by the interaction of two KAWs. Neglecting the toroidal coupling term on the right-hand side, Eq. (1) describes a KAW, which is propagating for $\Delta_1 > 0$ and evanescent for $\Delta_1 < 0$.[19] Toroidal effects couple together the poloidal harmonics 1 and 2. As shown in Fig. 2a, when the eigenvalue $\Delta < 0$, (true for the TAE) a small evanescent region separates the propagating regions. If this region is small enough, or if $|\hat{\tau}|$ is sufficiently large, the TAE excites a KAW on harmonic 1 which propagates away to the left and another KAW on harmonic 2 which propagates away to the right. As long as $\mathrm{Im}(\hat{\tau})$ is finite, the KAWs will damp and not be reflected back in this plane slab model. Consequently there is significant damping for vanishingly small $\mathrm{Im}(\hat{\tau})$.

The KTAE dispersion relation is found by replacing $\hat{\varepsilon}$ by $-\hat{\varepsilon}$ in Eqs. (30) and (31). The extremum that satisfies the constraints on the integrals is approximately

$$\lambda = [\hat{\tau}(\hat{\Delta} + \hat{\varepsilon})]^{1/2} \tag{38}$$

and gives the dispersion relation

$$\hat{\Delta} = \hat{\varepsilon} + \left[\frac{\hat{\tau}}{(\hat{\Delta} + \hat{\varepsilon})}\right]^{1/2} . \tag{39}$$

There are several differences between this mode and the TAE. First, the mode lies on the top side of the gap boundary, $\mathrm{Re}(\hat{\Delta}) > 0$. Second, the mode may be outside the gap,

$\mathrm{Re}(\hat{\Delta}^2) > \hat{\varepsilon}^2$. Third, the damping scales as $\hat{\tau}^{1/2}$. Equation (39) is plotted along with the code results in Fig. 1b. The $\hat{\tau}^{1/2}$ behavior for both are clearly seen, although there is a moderate increase in the slope of $\mathrm{Im}(\hat{\Delta})$ vs. $|\hat{\tau}|/\hat{\varepsilon}^3$ for $|\hat{\tau}|/\hat{\varepsilon}^3 \sim 0.1$ which is not represented in Eq. (39). This increased damping is due to the excitation of KAWs propagating away from the gap region, similar to that described for the TAE. In this case, however, the transition to this regime is not as strong. Since $\mathrm{Re}(\hat{\Delta}) > 0$, the KTAE is formed by the interaction of two KAWs as shown in Fig. 2b. Here, the propagating regions for harmonics 1 and 2 overlap. Apparently this situation is less favorable to the excitation of propagating KAWs than the TAE case. Perhaps the evanescent region in the TAE case forces out the KAW for $|\hat{\tau}|/\hat{\varepsilon}^3 > 1$ and causes the large damping. The damping of the KTAE is larger than the TAE for $|\hat{\tau}|/\hat{\varepsilon}^3 \ll 1$ due to the $\hat{\tau}^{1/2}$ scaling, but smaller than the TAE for $|\hat{\tau}|/\hat{\varepsilon}^3 \gtrsim 1$.

V. Numerical Results and Discussion

The dispersion relations given by Eqs. (33), (37), and (39) are valid if the symmetric wave function $\psi_s(y) = \psi_1(y) + \psi_1(-y)$ is relatively close to the assumed form $e^{-\lambda y^2/2}$. This was tested by direct numerical integration of the basic equations with a shooting code (originally developed by J. Sedlak). Our code solves the coupled system given by Eqs. (11a) and (11b) with the WKB-type boundary conditions

$$\frac{\psi_1}{\psi_2} = \frac{\{\pm i[\hat{\varepsilon}^2 - h^2(y)]^{1/2} - h(y)\}}{[\hat{\varepsilon}/f(y)]} \tag{40}$$

at $y \gg 1$ and $y \ll -1$ respectively. The code input $\hat{G}_1, \hat{G}_2, y_1^2, y_2^2, \hat{\tau}, \hat{\varepsilon}$, which are calculated from their definitions. The solutions are rapidly convergent and robust.

The numerical solutions discussed in Sec. IV and shown in Figs. 1a and 1b were calculated with the values $\hat{\varepsilon} = 0.1$, $\hat{G}_1 = 1.4$, $\hat{G}_2 = -0.35$, $y_1^2 = 0.5$, $y_2^2 = 2.0$, and $\mathrm{Arg}(\hat{\tau}) = -0.3$. These values reflect representative plasma parameters as shown in Table 1 and discussed below.

As a benchmark, we chose to run the code for TFTR device parameters under two quite different operating conditions. The first case corresponds to the TFTR TAE experiment discussed in Ref. 4. The second case corresponds to a D-T burning experiment. The plasma parameters for each case are shown in Table 1. In both cases the plasma density and q profiles were chosen to scale parabolically with r/r_p, while the temperature $T_e \sim [1 - (r/r_p)^2]^2$. An effective mass of 2.5 was assumed. For each case, we consider three sets of mode numbers: $n = (1,1)$, $m = (1,2)$ with $q = 1.5$; $n = (2,2)$, $m = (2,3)$ with $q = 1.25$; and $n = (3.3), m = (3.4)$ with $q = 1.17$. The $n = 2$ case fits the experimentally measured $q \sim 1.3$ of Ref. 4. In Table 1, the corresponding normalized parameters $\widehat{\varepsilon}$, $\widehat{G}_0$, and $\widehat{\tau}/\widehat{\varepsilon}^3$ are shown with the numerically computed eigenvalues for the TAE and KTAE and the damping coefficients γ/ω [calculated from Eq. (13)]. For comparison, corresponding values of $(\gamma/\omega)_{\rm mcd}$ due to the magnetic curvature drift of the electrons [calculated from Eq. (10) of Ref. 2] are also indicated.

We see from Table 1 that the numerically computed damping coefficients for the TAE are significantly (a factor of 5-15) higher than the Landau damping $(\gamma/\omega)_{\rm mcd}$ predicted by past perturbative approaches for $n = 2$ and $n = 3$. Fortuitously, our predicted damping coefficient for the TAE experiment for $n = 2$ is close to the experimentally measured value (of Ref. 4) of $\sim 3\%$. The damping is high in these cases because the normalized parameter $|\widehat{\tau}|/\widehat{\varepsilon}^3$ is near or greater than unity. Consequently, these cases are near or into the regime where the dispersion relation given by Eq. (37) is valid. In this regime, the damping is dominated by excitation of KAWs propagating away from the gap region. This indicates the importance of our non-perturbative approach. In contrast, for $n = 1$, we see that the numerically computed damping coefficients for the TAE are relatively close to the perturbative $(\gamma/\omega)_{\rm mcd}$. The damping is weaker in these cases because $|\widehat{\tau}|/\widehat{\varepsilon}^3 \ll 1$, which corresponds to the regime where the dispersion relation given by Eq. (33) is valid. The KTAE damping coefficients are nearly equal to those for the TAE for $n = 1$ and smaller than those for the TAE for $n = 2$ and

$n = 3$.

Figure 3a shows the $n = 2, m = 2$ TAE wave function $\psi_1(y)$ in normalized Fourier space for the D-T burning experiment (fifth column in Table 1). The oscillatory character is due to the influence of $\hat{\tau}$ and the connected excitation of the KAW. For $n = 1, m = 1$ (column 4), $\psi_1(y)$ has a significantly less oscillatory character due to the smaller value of $|\hat{\tau}|/\hat{\varepsilon}^3$. Figure 3b shows the perpendicular electric field $E_1(r/r_p)$ in real space corresponding to the inverse transform [Eqs. (8a) and (10a)] of $\psi_1(y)$. Oscillations to the left are a propagating KAW. This may be compared to the diagram of Fig. 2a. Figure 3c shows the perpendicular electric field $E_2(r/r_p)$ corresponding to the inverse transform [Eqs. (8a) and (10b)] of $\psi_2(y)(m = 3)$. Oscillations to the right are a propagating KAW. Note that E_1 and E_2 are in phase. For the KTAE, (not shown) it is interesting that E_1 and E_2 in real space are very similar to E_1 and E_2 for the TAE, although the oscillations are less prominent. The major difference is that E_1 and E_2 are *out* of phase.

Predictions of the $\hat{\Delta}/\hat{\varepsilon}$ from the dispersion relations given by Eqs. (33), (37), and (39) generally were found to lie within a factor of two of the values from the shooting code for the cases cited in Table 1. We comment that, for lower mode numbers ($m = 1, 2$), decreasing the value of $\hat{G}_0$ by $\sim 35\%$ from its definition $\hat{G}_0 = \frac{1}{2}(\hat{G}_1 + \hat{G}_2)$ is found to improve the prediction of Eq. (33). This is not unreasonable considering the approximations used in its derivation.

For higher mode numbers, the wave functions become more localized in real space. Damping coefficients generally become higher. For the TAE, this is due to an increase in the normalized parameter $|\hat{\tau}|/\hat{\varepsilon}^3$ with m to values greater than unity. Then the dispersion relation given by Eq. (37) holds. The damping coefficient in this case can be estimated by writing $\hat{\tau}/\hat{\varepsilon}^3$ in terms of the unnormalized parameters to leading order in ε (unnormalized) and combining Eqs. (37) and (13). The result is

$$\frac{\hat{\tau}}{\hat{\varepsilon}^3} = 8\frac{s^2}{(2\varepsilon)^3}\left(\frac{\rho_s}{r}\right)^2\sqrt{m_1 m_2}\,(m_1 + m_2)/F \tag{41}$$

$$\frac{\gamma}{\omega} = -3\left(\frac{m_1 m_2}{m_1+m_2}\frac{s}{2^{1/2}}\frac{\rho_s}{r}\right)^{2/3} \mathrm{Im}\left[i\left(\frac{i}{F}\right)^{1/3}\right] . \tag{42}$$

Note that $F \cong 1$ and therefore $\mathrm{Im}[i(i/F)^{1/3}] \cong 1$, even for vanishingly small $\mathrm{Im}(F)$. For $m_1 = n_1 = n_2 = m$ and $m_2 = m+1$, $q = 1+\frac{1}{2m}$ and, with a parabolic q profile $q = 1+(r/r_p)^2$, the shear $s = (r/r_p)(2/m)^{1/2}/(1+\frac{1}{2m})$. Then, in the high m limit, Eq. (42) becomes

$$\frac{\gamma}{\omega} = -3\left(\frac{\rho_s}{2r_p}\right)^{2/3} m^{1/3}\,\mathrm{Im}\left[i\left(\frac{i}{F}\right)^{1/3}\right] . \tag{43}$$

This equation gives surprisingly good agreement with the code results when $|\hat{\tau}|/\hat{\varepsilon}^3 \gtrsim 1$ and even for the $n = 1$ and $n = 3$ cases given in Table 1.

Finally we comment that for DIII-D, the kinetic effects on the TAE may be more significant than for TFTR because of larger shear.

VI. Conclusions

In conclusion, a non-perturbative treatment of electron parallel dynamics predicts a non-negligible combined collisional and collisionless (Landau) damping of the TAE. The damping rate for the TAE predicted in this study is of the same order as the resonant or continuum damping,[6–8] which is caused by a mechanism not treated in this study. Our theory points out the possible importance of a non-perturbative treatment of damping for the TAE. Although the form of damping examined in this study may not in itself be enough to overcome the α-particle drive, it should be taken into account in more careful future studies. Our theory also predicts the existence of a new TAE (the KTAE) which depends on finite conductivity and is formed by the coupling of two KAWs. Since the damping of these modes can be smaller than the TAE, a study of the effect of α-particles on these modes is also warranted.

Acknowledgments

We are grateful to David W. Ross, Wann-Quan Li, and Herbert L. Berk for helpful discussions and criticisms and to David M. Lindberg, Y.-Z. Zhang, and William H. Miner, Jr. for help

in computer programming. This work is funded in part by the U.S. Department of Energy Contract No. DE-FG05-80ET53088.

A. Conductivity Model

Our parallel conductivity model is derived by following the drift-tearing mode analysis of Chen, Rutherford and Tang.[16] This is reasonable since the essential features of the TAE mode structure are described by electrostatic potential φ and the parallel component of the magnetic vector potential A, as in the tearing mode. That $k \cong 0$ for the tearing mode does not affect the derivation of the conductivity. In this analysis, the perturbed electron distribution function h is determined by the drift-kinetic equation. Trapped (t) and passing (p) components are treated as separate species $h = h_t + h_p$ but are related to each other through the collision operator. The collision operator acting on the perturbed trapped particle distribution is modelled as

$$Ch_t = -\nu(v)\widehat{h}_t \ . \tag{A1}$$

It simply tells the rate of scatter of trapped electrons out of the trapped region. In this equation, the carat designates the non-Maxwellian part, while $\nu(v) = (\nu_e/\varepsilon)(v_e/v)^3$, where ν_e is the collision frequency of thermal electrons on the ions and v_e is the electron thermal speed. [The quantity (ν_e/ε) represents the effective collision rate of the trapped electrons out of the trapped region.] The collision operator acting on the perturbed passing electron distribution is modelled as

$$Ch_p = \frac{f_0}{n_{0p}} \int_t d^3v \nu(v) \widehat{h}_t - \nu_p \left[h_p - \frac{f_0}{n_{0p}} \int_p d^3v h_p \right] \ . \tag{A2}$$

The first term describes the rate of scatter of the trapped electrons into the passing region. Here, f_0 and n_0 represent the unperturbed distribution function and density. The second term is added to the analysis of Chen, Rutherford and Tang. This term is a particle-conserving Krook collision operator where ν_p is an effective collision frequency for the passing electrons on the ions. For simplicity, ν_p is taken to be a constant in our analysis. We take

$\nu_p = \nu_e(v_e/v_A)^3$ to account for the importance of the resonance $\omega = kv_A$ in the drift-kinetic equation for the passing particles. We comment that a velocity dependence $\nu_p(v)$ results in an integral equation for h_p that is not readily solved. Trapping and collisional effects of the ions are neglected.

Relationships between the perturbed electron distributions h_p and h_t and the fields φ and A are obtained by substituting Eqs. (A1) and (A2) into the drift-kinetic equation and bounce-averaging. (For simplicity, no distinction is made between φ and A and their bounce-average values. We also take $\omega_*/\omega \to 0$.) From the total electron and ion distribution functions, we obtain density and current perturbations which are substituted into the quasineutrality condition and Amperé's law. The parallel conductivity is extracted from the resulting coupled equations for the fields φ and A.

References

1. C.Z. Cheng and M.S. Chance, Phys. Fluids **29**, 3695 (1986).

2. G.Y. Fu and J.W. Van Dam, Phys. Fluids B **1**, 1949 (1989).

3. C.Z. Cheng, Phys. Fluids B **3**, 2463 (1991).

4. K. L. Wong, R. J. Fonck, S. F. Paul, D. R. Roberts, E. D. Fredrickson, R. Nazikian, H. K. Park, M. Bell, N. L. Bretz, R. Budny, S. Cohen, G. W. Hammett, F. C. Jobes, D. M. Meade, S. S. Medley, D. Mueller, Y. Nagayama, D. K. Owens, and E. J. Synakowski, Phys. Rev. Lett. 66, 1874 (1991).

5. W. W. Heidbrink, E. J. Strait, E. Doyle, G. Sager, and R. T. Snider, Nuc. Fusion 31, 1635 (1991).

6. F. Zonca and L. Chen, Phys. Rev. Lett. **68**, 592 (1992).

7. M.N. Rosenbluth, H.L. Berk, J.W. Van Dam, and D.M. Lindberg, Phys. Rev. Lett. **68**, 596 (1992).

8. H.L. Berk, J.W. Van Dam, Z. Guo, and D.M. Lindberg, "Continuum damping of low-n toroidicity-induced shear Alfvén eigenmodes," submitted to Phys. Fluids B.

9. N.N. Gorelenkov and S.E. Sharapov, Physica Scripta **45**, 163 (1992).

10. S.M. Mahajan, Phys. Fluids **27**, 2238 (1984).

11. D. M. Meade, V. Arunasalam, C. W. Barnes, M. G. Bell, R. Bell, M. Bitter, R. Boivin, N. L. Bretz, R. Budny, C. E. Bush, A. Cavallo, C. Z. Cheng, T. K. Chu, S. A. Cohen, S. Cowley, S. L. Davis, D. L. Dimock, J. Dooling, H. F. Dylla, P. C. Efthimion, A. B. Ehrhardt, R. J. Fonck, E. D. Fredrickson, H. P. Furth, R. J. Goldston, G. J. Greene, B.

Grek, L. R. Grisham, G. W. Hammett, R. J. Hawryluk, K. W. Hill, J. C. Hosea, R. B. Howell, H. Hsuan, R. A. Hulse, A. C. Janos, D. L. Jassby, F. C. Jobes, D. W. Johnson, L. C. Johnson, R. Kaita, S. M. Kaye, J. Kesner, C. Kieras-Phillips, S. J. Kilpartick, H. Kugel, P. H. LaMarche, B. LeBlanc, D. M. Manos, D. K. Mansfield, E. S. Marmar, M. E. Mauel, E. Mazzucato, M. P. McCarthy, D. C. McCune, K. M. McGuire, S. S. Medley, D. R. Mikkelsen, D. A. Monticello, R. W. Motley, D. Mueller, J. Murphy, Y. Nagayama, G. A. Navratil, R. Nazikian, D. K. Owens, H. K. Park, W. Park, S. F. Paul, R. Perkins, S. Pitcher, A. T. Ramsey, M. H. Redi, G. Rewoldt, D. R. Roberts, A. L. Roquemore, P. H. Rutherford, S. A. Sabbagh, G. Schilling, J. Schivell, G. L. Schmidt, S. D. Scott, J. Snipes, J. E. Stevens, W. Stodiek, B. C. Stratton, E. J. Synakowski, W. M. Tang, G. Taylor, J. L. Terry, J. R. Timberlake, H. H. Towner, M. Ulrickson, S. Von Goeler, R. M. Wieland, M. Williams, J. R. Wilson, K. L. Wong, M. Yamada, S. Yoshikawa, K. M. Young, M. C. Zarnstorff, and S. J. Zweben in Proceedings of the Thirteenth International Conference on Plasma Phyics and Controlled Nuclear Fusion Research, Washington, D. C., 1990 (International Atomic Energy Agency, Vienna, 1991).

12. DIII-D team (F. W. Baity, H. Biglari, G. Bramson, J. N. Brooks, N. H. Brooks, D. Buchenauer, K. H. Burrell, J. D. Callen, R. W. Callis, T. N. Carlstrom, C. Challis, V. Chan, M. S. Chance, Z. Chang, M. S. Chu, S. Coda, A. P. Colleraine, J. C. DeBoo, J. C. DeGentile, J. DeHaas, P. H. Diamond, I. Doi, R. Dominguez, E. J. Doyle, H. Duong, R. F. Ellis, J. R. Ferron, T. K. Fowler, R. L. Freeman, T. Fukuda, A. Futch, A. Fyaretdinov, G. Giruzzi, P. Gohil, Y. Gorelov, R. Goulding, C. M. Greenfield, R. J. Groebner, G. Haas, R. Harvey, W. Heidbrink, D. N. Hill, F. L. Hinton, D. J. Hoffman, J. Hogan, R. Hong, W. Howl, C. L. Hsieh, W. L. Hsu, G. L. Jackson, R. A. James, S. Janz, T. Jarboe, T. Jensen, R. Jong, Y. Kamada, A. G. Kellman, J. Kim, C. C. Klepper, H. Kubo, T. Kurkio-Suonio, R. LaHaye, L. L. Lao, E. A. Lazarus, R. Lee, T.

Lehecka, B. Leikind, S. I. Lippmann, J. Lister, B. Lloyd, J. M. Lohr, T. C. Luce, N. C. Luhmann, Jr., J. L. Luxon M. A. Mahdavi, K. Matsuda, H. Matsumoto, G. Matthews, M. Mayberry, M. Menon, B. Mills, P. Mioduszewski, C. P. Moeller, T. Ohkawa, T. Okazaki, T. H. Osborne, D. O. Overskei, L. Owen, W. A. Peebles, P. I. Petersen, T. W. Petrie, C. Petty, R. Philipona, J. Phillips, R. Pinsker, P. A. Politzer, M. Porkolab, G. D. Porter, R. Prater, M. E. Rensink, C. Rettig, T. Rhodes, J. Rodriguez, M. N. Rosenbluth, G. Sager, M. Saigusa, M. J. Schaffer, D. P. Schissel, L. Schmitz, J. T. Scoville, R. P. Seraydarian, T. C. Simonsen, R. T. Snider, G. M. Staebler, B. W. Stallard, R. D. Stambaugh, R. Stav, H. St. John, R. E. Stockdale, E. J. Strait, W. Tang, P. L. Taylor, T. S. Taylor, P. K. Trost, V. Trukhin, A. Turnbull, R. Waltz, J. Watkins, J. Wright, J. Winter, and D. Wroblewski) in Proceedings of the Thirteenth International Conference on Plasma Phyics and Controlled Nuclear Fusion Research, Washington, D. C., 1990 (International Atomic Energy Agency, Vienna, 1991).

13. S.M. Mahajan, D.W. Ross, and G-L. Chen, Phys. Fluids **26**, 2195 (1983).

14. Y-M. Li, S.M. Mahajan, and D.W. Ross, Phys. Fluids **30**, 1466 (1987).

15. D.W. Ross, G.L. Chen, and S.M. Mahajan, Phys. Fluids **25**, 652 (1982).

16. L. Chen, P.H. Rutherford, and W.M. Tang, Phys. Rev. Lett. **39**, 460 (1977).

17. S.M. Mahajan, R.D. Hazeltine, H.R. Strauss, and D.W. Ross, Phys. Fluids **22**, 2147 (1979).

18. I.S. Gradshteyn and I.M. Ryzhik, *Table of Integrals, Series and Products*, 4th ed. (Academic Press, New York, 1980).

19. A. Hasegawa and L. Chen, Phys. Rev. Lett. **35**, 370 (1975).

TABLE 1 - eigenvalues, damping rates, and other parameters

	TAE exp			*D-T exp*		
r_p(m)	0.75			0.8		
R(m)	2.4			2.5		
T_e(KeV)	1.7			10		
n(cm^{-3})	2.7×10^{13}			10^{14}		
B(T)	1.1			5		
q_{cntr}	1.04			1.04		
q_{edge}	2.8			3.1		
n | m	(1, 1) | (1, 2)	(2, 2) | (2, 3)	(3, 3) | (3, 4)	(1, 1) | (1, 2)	(2, 2) | (2, 3)	(3, 3) | (3, 4)
$\hat{\varepsilon}$	0.131	0.161	0.194	0.124	0.153	0.183
$\hat{G}_0$	0.504	0.164	8.28×10^{-2}	0.505	0.163	8.13×10^{-2}
Arg($\hat{\tau}$)	−0.583	−0.478	−0.448	−0.240	−0.187	-0.178
$\lvert\hat{\tau}\rvert/\hat{\varepsilon}^3$	8.57×10^{-2}	0.689	2.10	3.77×10^{-2}	0.268	0.79
$(\hat{\Delta}/\hat{\varepsilon})_{\text{TAE}}$	$-0.75 - 0.079i$	$-0.96 - 0.50i$	$-0.98 - 0.97i$	$-0.75 - 0.031i$	$-0.92 - 0.29i$	$-0.93 - 0.57i$
$(\hat{\Delta}/\hat{\varepsilon})_{\text{KTAE}}$	$1.4 - 0.10i$	$1.8 - 0.22i$	$2.2 - 0.43i$	$1.3 - 0.030i$	$1.5 - 0.053i$	$1.8 - 0.12i$
$(\gamma/\omega)_{\text{TAE}}$	-1.2×10^{-2}	-5.3×10^{-2}	-8.0×10^{-2}	-4.4×10^{-3}	-2.9×10^{-2}	-4.5×10^{-2}
$(\gamma/\omega)_{\text{KTAE}}$	-1.6×10^{-2}	-2.3×10^{-2}	-3.5×10^{-2}	-4.3×10^{-3}	-5.3×10^{-3}	-9.1×10^{-3}
$(\gamma/\omega)_{mcd}$	-3.7×10^{-3}	-4.8×10^{-3}	-5.2×10^{-3}	-4.1×10^{-3}	-5.1×10^{-3}	-5.4×10^{-3}

Figure Captions

1. Comparison of analytic dispersion relations with numerical shooting code results. Solid lines indicate real part and dashed lines the negative imaginary part. a) $(\widehat{\Delta}/\widehat{\varepsilon}+1)$ vs. $|\widehat{\tau}|/\widehat{\varepsilon}^3$: The labels "$C$" "33," and "37" designate code results, Eq. (33) and Eq. (37), respectively. b) $(\widehat{\Delta}/\widehat{\varepsilon}-1)$ vs. $|\widehat{\tau}|/\widehat{\varepsilon}^3$: The labels "$C$" and 39 designate code results and Eq. (39), respectively.

2. Superimposed plots of Δ_1 and Δ_2 in real space near the gap indicating regions of propagating and evanescent KAWs. a) TAE case. b) KTAE case.

3. Wave functions from the numerical shooting code corresponding to the D-T burning case $n=(2,2)$ and $m=(2,3)$ in Table 1. a) Wave function $\psi_1(y)(m=2)$ in normalized Fourier space. b) Perpendicular electric field corresponding to the inverse transform [Eqs. (8a) and (10a)] of $\psi_1(y)$. Oscillations to the left are due to a propagating KAW. c) Perpendicular electric field corresponding to the inverse transform [Eqs. (8a) and (10b)] of $\psi_2(y)(m=3)$. Oscillations to the right are due to a propagating KAW.

a) TAE

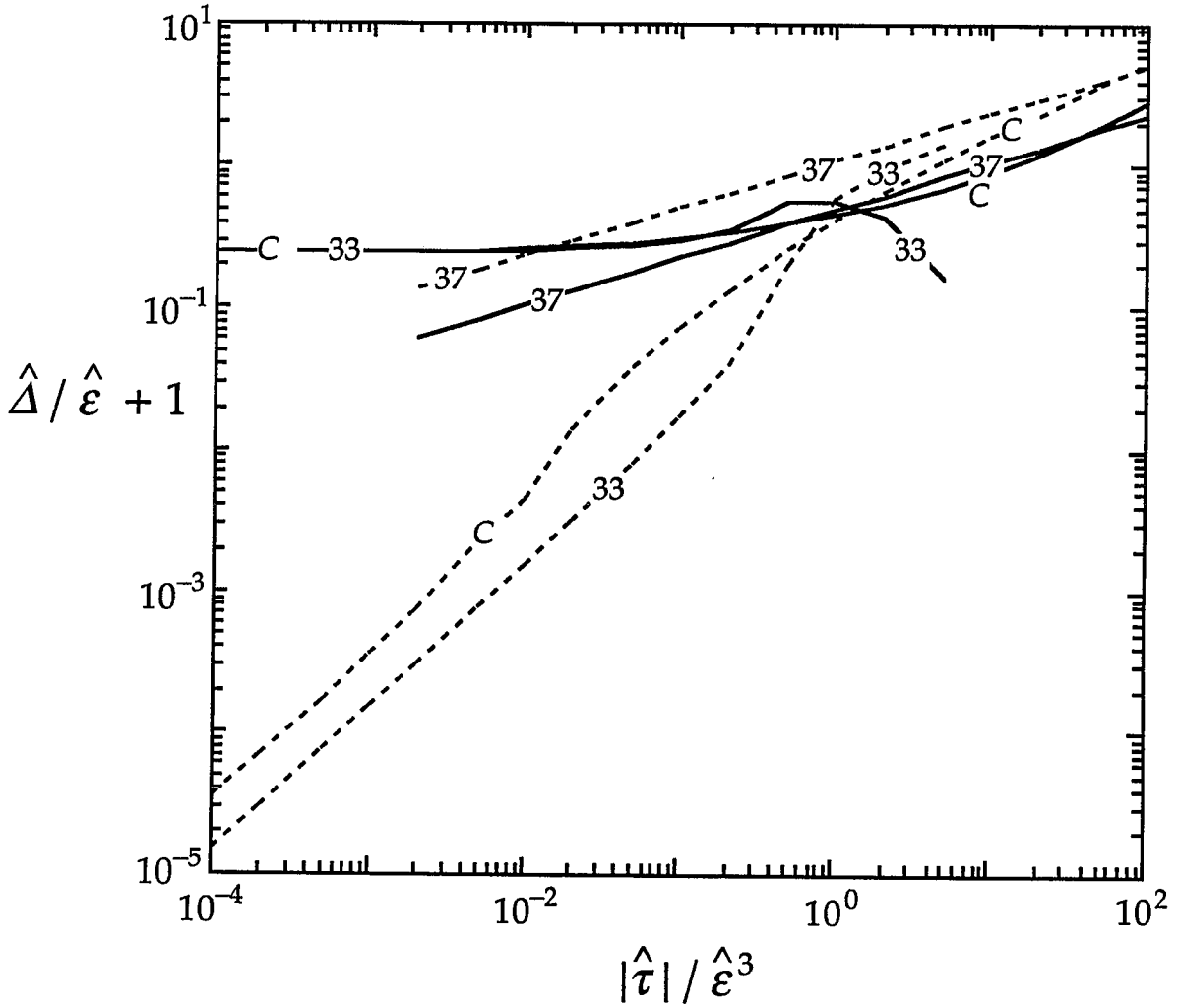

Fig. 1a Mett PF-19251

b) KTAE

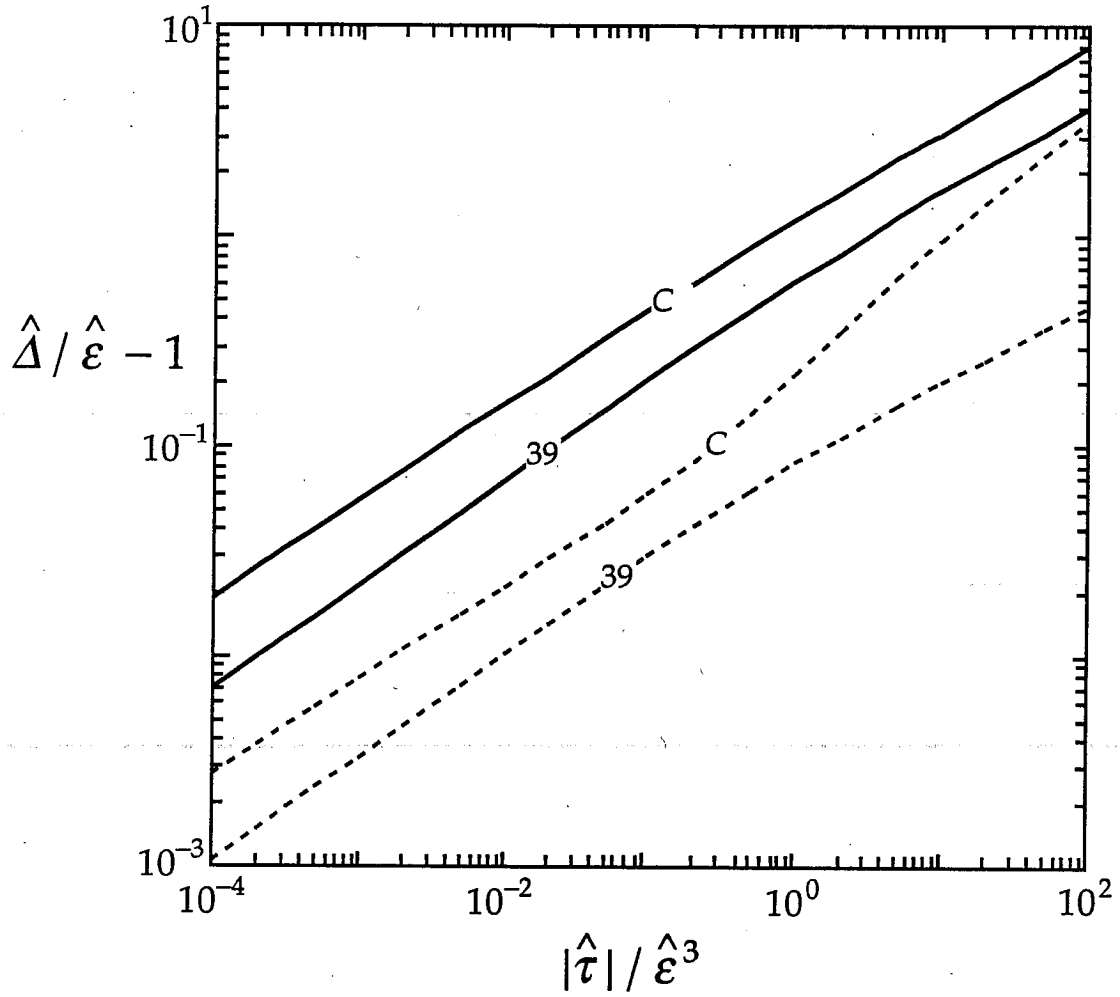

Fig. 1b Mett PF-19251

a) TAE

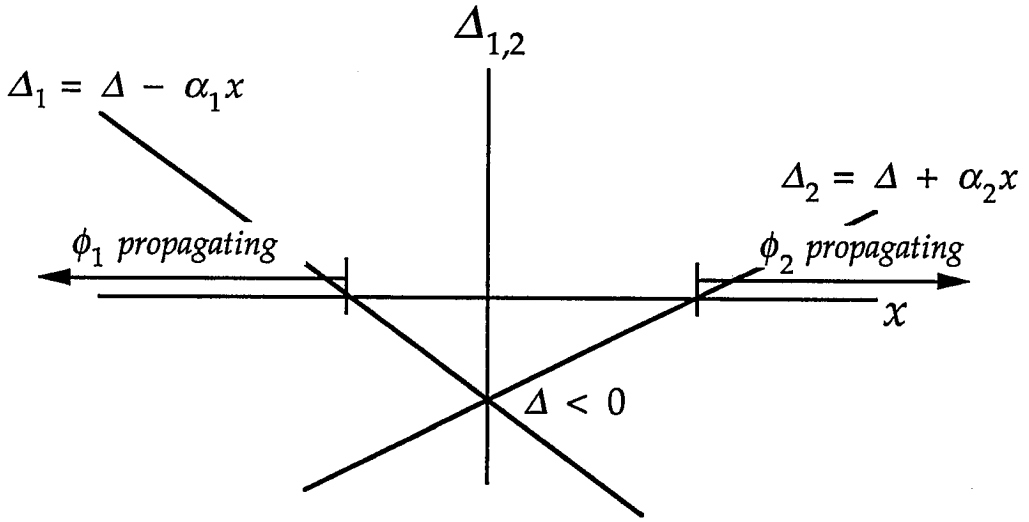

b) KTAE

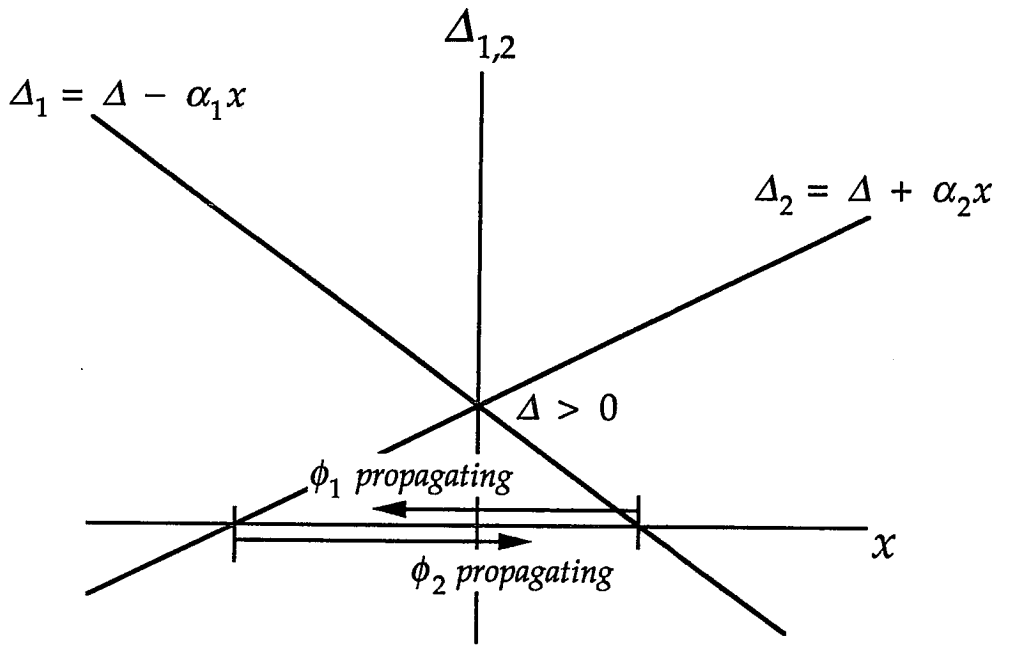

Fig. 2 Mett PF-19251

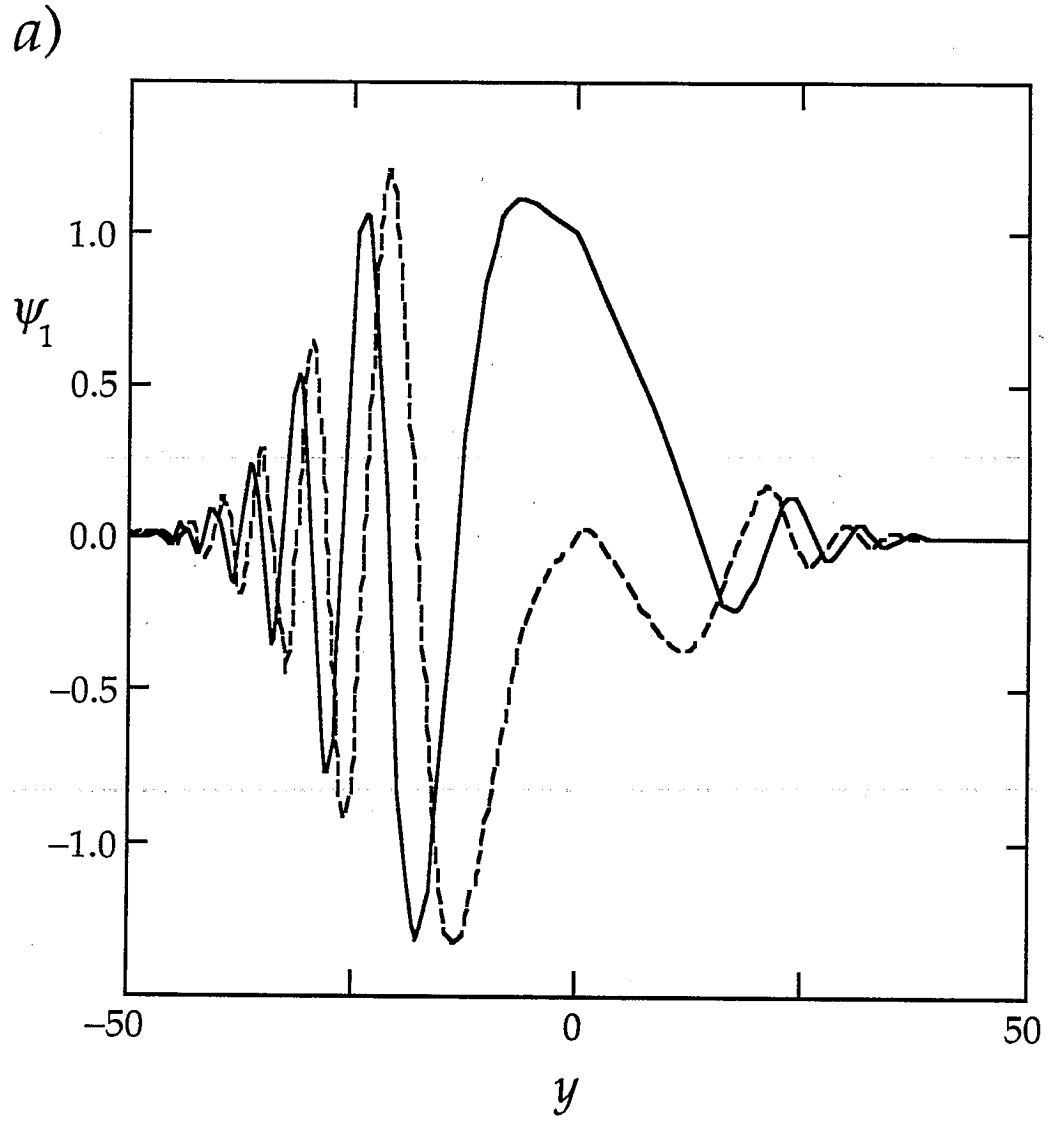

Fig. 3a Mett PF-19251

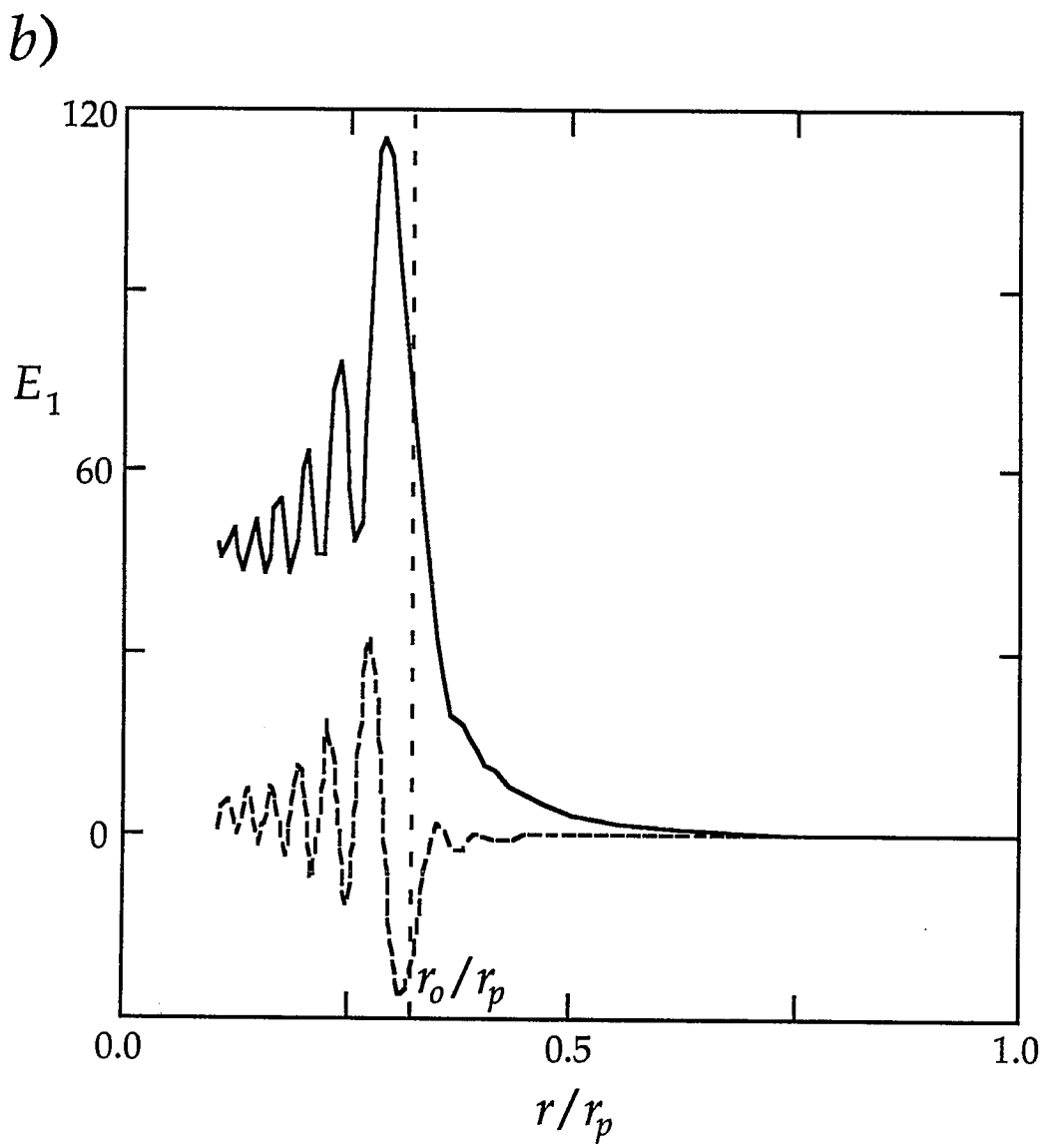

Fig. 3b Mett PF-19251